# High-Order Cross Section Homogenization Method

Farzad Rahnema and Michael Scott McKinley

Georgia Institute of Technology
Nuclear Engineering and Health Physics Programs
*The George W. Woodruff School of Mechanical Engineering*
*Atlanta, GA 30332-0405 USA*
Email: *farzad.rahnema@me.gatech.edu and mckinley9@llnl.gov*

Number of Pages: 25 **(**including this page)
Number of Tables: 17
Number of Figures: 8

Send correspondences to:

Farzad Rahnema
Georgia Institute of Technology
Nuclear Engineering and Health Physics Programs
The George Woodruff School of Mechanical Engineering
Atlanta, GA 30332-0405
Voice: (404) 894-3731
Fax: (404) 894-3733
E-mail: farzad.rahnema@me.gatech.edu

# High-Order Cross Section Homogenization Method

Farzad Rahnema and Michael Scott McKinley

Georgia Institute of Technology
Nuclear Engineering and Health Physics Programs
*The George W. Woodruff School of Mechanical Engineering*
*Atlanta, GA 30332-0405 USA*
Email: farzad.rahnema@me.gatech.edu and gt1623c@prism.gatech.edu

**Abstract –** *A high-order cross section homogenization method based on boundary condition perturbation theory is developed to improve the accuracy of nodal methods for coarse-mesh eigenvalue calculations. The method expands the homogenized parameters such as the cross sections and the neutron flux discontinuity factor in terms of the node surface current-to-flux ratio. The expansion coefficients are evaluated during the nodal calculations using additional precomputed homogenization parameters. As a result, it is possible to correct (update) the homogenized parameters to arbitrary order of accuracy for the effect of reactor core environment (fuel assembly neutron leakage) with very little computational effort in the core calculation. The reconstructed fine-mesh flux (fuel- pin power) is a natural byproduct of the new method. A benchmark problem typical of a BWR core is analyzed in one dimension, monoenergetic diffusion theory by modifying a nodal method based on a bilinear, flat as well as a fine-mesh intranodal flux shape. The homogenized parameters are first computed using exact (fine-mesh) albedos and compared to those determined from a fine-mesh core calculation. Two nodal (coarse-mesh) examples are given to show how well this approach works as a higher-order perturbation method is utilized. The paper concludes by showing that this method succeeds in giving excellent results for cores that may be difficult to model using standard nodal methods.*

## I. INTRODUCTION

Modern nodal methods are used as standard tools for design and monitoring of light water reactor (LWR) cores. See Lawrence (1986) for a review of these methods. A major contributor to the success of these methods is the homogenization and dehomogenization (fuel-pin flux and power reconstruction) techniques (Koebke, 1978 and 1981 and Smith, 1986). In recent years, considerable effort has been spent in the development of nodal (homogenized) cross sections that account for both the spatial and depletion history effects (Lindahl and Muller, 1996, Forslund, Muller & Lindahl, 2000, Grummer, Lewis and Merk, 1997, Moon, 1997, Iwamoto and Yamamoto, 1998, Wagner and Koebke 1981, Palmtag and Smith, 1998, Mori and Kawamura, 1995, Chao and Shatilla, 1998, Smith, 1994, Rahnema and Nichita, 1997, Vogel and Weiss, 1992, Lee, Kim, Song and Park, 1996, Yan, 1999, Rajic and Ougouag, 1988). These methods compensate to various degrees for deficiencies inherent in the standard nodal cross section generation process based on single assembly (SA) lattice depletion calculations using reflective boundary conditions and selective depletion history conditions which may not be representative of the actual core condition.

Nodal methods based on generalized equivalence theory (Smith, 1986), GET, use homogenized cross sections and discontinuity factors for each node (fuel assembly) that are determined by performing single assembly fine-mesh calculations with no net neutron leakage (zero-current or current-to-flux ratio boundary condition). These are referred to as infinite medium homogenized parameters. It is known that for configurations in which the node-to-node neutron leakage is large, the use of infinite medium parameters, especially the discontinuity factor, could lead to large errors in the nodal solution (Rahnema and Nichita, 1997). This would be the case for highly heterogeneous core configurations of modern reactor designs, mixed oxide (MOX) as well as small reactor cores (in terms of mean free path).

In the terminology of perturbation theory, the infinite medium homogenized parameters have $0^{th}$ order accuracy. Smith (1994) introduced the technique of "rehomogenization." In this method, the homogenized cross sections are recomputed at each power (or cross section reevaluation) iteration by assuming that the intranodal heterogeneous flux can be obtained by modulating the heterogeneous zero-current shape from the latest assembly calculation with the homogeneous (nodal) shape. This procedure is simple to implement and it does not require any supplementary assembly calculation. However, it cannot be used to correct the discontinuity factor. This is a serious drawback of the method since it has been shown (Rahnema and Nichita, 1997) that correcting only the cross sections without correcting the discontinuity factor is inconsistent and may actually reduce accuracy. Rahnema and Nichita (1997) introduced a leakage corrected spatial homogenization technique to account for the leakage effect on the homogenized parameters including the discontinuity factor. The improvement was achieved through the use of a first-order fitting technique in which it was assumed that the homogenized parameters are linear functions of node boundary current-to-flux ratio. This method is equivalent to a first-order perturbation method and therefore has limited applicability in the case of highly heterogeneous systems.

Recently, a heterogeneous finite element method (Nichita and Rahnema, 1998) was developed for coarse-mesh core calculations. The method, which does not use homogenized cross sections, is a Lagrange finite element method that uses basis functions that include the fine-mesh detail. The elementary basis functions are generated from fixed boundary flux fine-mesh (heterogeneous) assembly calculations. The method is as accurate as nodal methods for mildly heterogeneous cores and more accurate for highly heterogeneous cores. Its main drawback is that the basis functions are dependent on an assumed core multiplication factor that is not known a priori (at the time of the fixed source calculation). Thus, its accuracy depends on how close the assumed $k_{eff}$ is to the actual core eigenvalue. Two other finite element methods (Ellison and Lewis, 1983, Calabrese and Grant, 1993) also use basis functions that include fine-mesh details. Calabrese and Grant (1993) use fine-mesh eigenvalue calculations to generate the basis functions. Non-zero boundary current-to-flux ratios are selected to force the eigenvalue calculations to yield the assumed core $k_{eff}$. The method has three drawbacks: 1) the computational time for the basis function calculation is quite large since eigenvalue problems are solved; 2) the method for generating the basis functions cannot be applied to non-multiplying nodes such as water (reflector) nodes; 3) the accuracy of the method, as in Nichita and Rahnema (1998), depends on how well the unknown core $k_{eff}$ is predicted (guessed). Ellison and Lewis (1983) assume that the fission source corresponding to the elementary basis functions is separable into the product of the zero-current assembly shape and the regular finite element polynomials. The method yields accurate results in mildly heterogeneous cores. However, as the heterogeneity (node-to-node leakage) increases, the separability assumption breaks down and, as a result, the errors increase.

Therefore, it would be highly desirable to develop a coarse-mesh method that, unlike the current nodal or finite element methods, is consistently accurate regardless of the degree of the heterogeneity of the fuel assembly or the reactor core. It is also desirable for the method not to require a priori knowledge of any core parameters such as $k_{eff}$ (the current limitation of the advanced finite element methods) or the single assembly boundary condition.

All applications that use boundary condition perturbation (Rahnema and Nichita, 1997) or rehomogenization (Smith, 1994) methods have generally been restricted to a first-order analysis. Recently, the first-order perturbation method of Rahnema (1989) has been extended to higher-order theory (McKinley and Rahnema, 2000). The new theory allows for the computation of the flux, eigenvalue, and homogenized cross sections up to any order by using two adjoint functions.

In this paper, we present a high-order homogenization method based on high-order boundary condition perturbation theory. The technique when applied to a nodal method within the context of GET reproduces results that are close to that of the fine-mesh (exact) solution based on the one-dimensional one-speed benchmark problems considered regardless of the intranodal flux shape. Two flux shapes were considered, namely flat and bilinear, to demonstrate this. The high-order homogenization method allows for the reconstruction of the fuel-pin flux and power distributions since the perturbation theory calculates the heterogeneous flux and cross sections up to an arbitrary order. For the purpose of comparison, results based on a "best fit" (fine-mesh homogenized node) intranodal flux shape are included to represent the most accurate nodal method using the standard GET homogenized cross sections (based on the single assembly infinite lattice calculations).

## II. METHOD

In this work, we use the method of McKinley and Rahnema (2000) to achieve homogenized parameter accuracy of arbitrary ($n^{\text{th}}$) order. In their work a high-order boundary condition perturbation method was developed for an arbitrary ratio of linear functionals of the solution in diffusion theory. This functional can be formulated to estimate the homogenized group cross section ($\sigma_{xg}$) and heterogeneous discontinuity factor in group $g$, $\chi_g$, (Rahnema and Nichita, 1997) as a function of the nodal boundary current-to-flux ratios ($\gamma$) as given below:

$$\sigma_{xg} \equiv \frac{\int_g dE \int_V d^3x \sigma_{xg}(\vec{r})\overline{\varphi}(\vec{r})}{\int_g dE \int_V d^3x \overline{\varphi}(\vec{r})} \equiv \frac{<\sigma_x(\vec{r})\overline{\varphi}(\vec{r})>_{\vec{x},g}}{<\overline{\varphi}(\vec{r})>_{\vec{x},g}} = \sigma_{xgo} + \varepsilon\sigma_{x1} + \varepsilon^2\sigma_{xg2} + \cdots + \varepsilon^n\sigma_{xgn} + O(\varepsilon^{n+1}) \quad (1)$$

$$\chi_g \equiv \frac{\int_g dE \int_S d^2x \overline{\varphi}(\vec{r})}{\int_g dE \int_V d^3x \overline{\varphi}(\vec{r})} = \chi_{go} + \varepsilon\chi_{g1} + \varepsilon^2\chi_{g2} + \cdots + \varepsilon^n\chi_{gn} + O(\varepsilon^{n+1}) \quad (2)$$

In the above equations, we see the expansion of the homogenized parameters in terms of a smallness parameter, $\varepsilon$. The variable, $\vec{r}$, represents the phase space (energy $E$ and position $\vec{x}$ variables) and $\overline{\varphi}$ is the normalized heterogeneous (fine-mesh) flux solution to the single assembly problem with $\varepsilon\gamma$ as the boundary current-to-flux ratio. (Note that the parameter $\varepsilon$ is used to emphasize the degree (order) of smallness. For example, $\varepsilon$ in $\varepsilon\gamma$ indicates that $\gamma$ is a first-order term.) The symbol $V$ is the assembly volume and $S$ or $\partial V$ is the surface bounding $V$. The brackets imply phase space integration with or without the subscript $\vec{r}$. The subscript $\vec{x}$ implies integration over the volume $V$ and the subscript $S$ implies that the spatial integration is over the surface of the system. The subscript $g$ implies an energy integration over the group width $E_g < E < E_{g-1}$. The flux is normalized such that its phase space integration is equal to one. The term on the right hand side of Eqs. (1) and (2) are functions of the boundary current-to-flux ratio and of equal or lower order perturbation terms. The subscript $x$ refers to the reaction type. From the work by McKinley and Rahnema (2000), we may determine these homogenized parameters to any accuracy with just the infinite medium fine-mesh solution and the boundary current-to-

flux ratio. The method requires two infinite medium adjoint functions (to be discussed later) that are precomputed together with the standard (infinite medium) GET homogenized parameters. Given these adjoints functions, one then updates (correct) the standard GET parameters ($\sigma_{xo}$ and $\chi_o$) by evaluating simple integrals during the nodal (core) calculation.

The homogenized cross section updating process in the nodal method is as follows. First, the nodal calculation is first performed using the standard (i.e. $\gamma = 0$, $n$ = 0) homogenization parameters. The solution from this calculation is then used to compute the node interface current-to-flux ratio $\gamma$ for each boundary on each node. Given the known (precomputed) initial infinite medium fine-mesh coefficients[1] and the resulting $\gamma$, higher-order boundary condition formalism is used to evaluate the updated homogenized parameters. The core calculation is then performed again with the updated parameters to determine the new $\gamma$'s. The iteration on the updating of the parameters is continued until convergence is achieved. As observed by Rahnema and Nichita (1997), only a few iterations are usually required for convergence of the homogenized parameters. We emphasize that since the adjoint functions are precomputed by perturbation theory, the cross section iteration in the core calculation involves evaluation of just simple integrals and therefore is completely decoupled from the assembly calculations. In addition, this method has the advantage that the reconstructed flux comes naturally through the use of precomputed adjoint Green's functions.

## III. DEVELOPMENT

Expanding the eigenvalue and flux with a smallness parameter, $\varepsilon$, as

$$\lambda = \lambda_o + \varepsilon\lambda_1 + \varepsilon^2\lambda_2 \cdots + \varepsilon^n\lambda_n + O(\varepsilon^{n+1}) \tag{3}$$

and

$$\overline{\varphi} = \overline{\varphi}_o + \varepsilon\overline{\varphi}_1 + \varepsilon^2\overline{\varphi}_2 \cdots + \varepsilon^n\overline{\varphi}_n + O(\varepsilon^{n+1}) \tag{4}$$

allows for each term to be computed as shown by McKinley and Rahnema (2000):

$$\lambda_1 = \frac{<\overline{\varphi}_o^* \gamma \overline{\varphi}_o>_s}{<\overline{\varphi}_o^* F \overline{\varphi}_o>} \tag{5a}$$

$$\lambda_2 = \frac{<\overline{\varphi}_o^* \gamma \overline{\varphi}_1>_s - \lambda_1 <\overline{\varphi}_o^* F \overline{\varphi}_1>}{<\overline{\varphi}_o^* F \overline{\varphi}_o>} \tag{5b}$$

$$\lambda_n = \frac{<\overline{\varphi}_o^* \gamma \overline{\varphi}_{n-1}>_s - \lambda_1 <\overline{\varphi}_o^* F \overline{\varphi}_{n-1}> - \lambda_2 <\overline{\varphi}_o^* F \overline{\varphi}_{n-2}> \cdots - \lambda_{n-1} <\overline{\varphi}_o^* F \overline{\varphi}_1>}{<\overline{\varphi}_o^* F \overline{\varphi}_o>}, \quad n > 2 \tag{5c}$$

and

[1] The adjoint functions from the infinite medium fine-mesh (single assembly) case is precomputed as additional homogenization parameters.

$$\overline{\varphi}_1(\vec{x}_o, E_o) = \frac{- < \Psi_o^* \gamma \varphi_o >_s}{< \varphi_o(\vec{x}) >} \tag{6a}$$

$$\overline{\varphi}_2(\vec{x}_o, E_o) = \lambda_1 < \Psi_o^* F \overline{\varphi}_1 > - < \Psi_o^* \gamma \overline{\varphi}_1 >_s \tag{6b}$$

$$\overline{\varphi}_n = \lambda_1 < \Psi_o^* F \overline{\varphi}_{n-1} > + \lambda_2 < \Psi_o^* F \overline{\varphi}_{n-2} > \cdots + \lambda_{n-1} < \Psi_o^* F \overline{\varphi}_1 > - < \Psi_o^* \gamma \overline{\varphi}_{n-1} >_s, \; n > 2 . \tag{6c}$$

The expression are derived by first expanding the system governing equation, $H\overline{\varphi} = \lambda F \overline{\varphi}$, with Eqs. (3) and (4) and equating terms of equal power of $\varepsilon$. These equations can be multiplied by an adjoint equation and integrated over phase space. Applying the definition of the adjoints, the equations can be simplified into the forms given in Eqs. (5) and (6).

In the above equations, $\overline{\varphi}_o^*$ is the standard adjoint function as defined in McKinley and Rahnema (2000) and $\Psi_o^*$ is a Green's function adjoint that is the solution to the standard adjoint diffusion equation with a delta-function plus the forward solution as the source in space and energy. The boundary conditions for the adjoint problems are the same as for the unperturbed forward problem, namely, a zero boundary current-to-flux ratio. The parameter $\lambda_n$ and $\overline{\varphi}_n$ are the $n^{th}$ order eigenvalue and normalized flux, respectively, and $F$ is the fission operator. The brackets $< .,. >$ indicate integration of the arguments over the phase space. A subscript "s" outside the brackets implies that the spatial integration is over the external surface of the region. The solution is found to the $n^{th}$ order by first solving for the $1^{st}$ order eigenvalue and then the normalized flux. For each perturbation order, solve for the flux and eigenvalue and then proceed to the next perturbation order. This algorithm has the advantage of recreating the flux as homogenization parameters are solved for. The multigroup homogenization parameters may then be taken from McKinley and Rahnema (2000) as:

$$\sigma_{o,g} = \frac{< \sigma(\vec{x}, E) \overline{\varphi}_o(\vec{x}, E) >_{\vec{x},g}}{< \overline{\varphi}_o(\vec{x}, E) >_{\vec{x},g}} \tag{7a}$$

$$\sigma_{1,g} = \frac{< \sigma(\vec{x}, E) \overline{\varphi}_1(\vec{x}, E) >_{\vec{x},g} - \sigma_{o,g} < \overline{\varphi}_1(\vec{x}, E) >_{\vec{x},g}}{< \overline{\varphi}_o(\vec{x}, E) >_{\vec{x},g}} \tag{7b}$$

$$\sigma_{2,g} = \frac{< \sigma(\vec{x}, E) \overline{\varphi}_2(\vec{x}, E) >_{\vec{x},g} - \sigma_{o,g} < \overline{\varphi}_2(\vec{x}, E) >_{\vec{x},g} - \sigma_{1,g} < \overline{\varphi}_1(\vec{x}, E) >_{\vec{x},g}}{< \overline{\varphi}_o(\vec{x}, E) >_{\vec{x},g}} \tag{7c}$$

$$\vdots$$

$$\sigma_{n,g} = \frac{< \sigma(\vec{x}, E) \overline{\varphi}_n(\vec{x}, E) >_{\vec{x},g} - \sigma_{o,g} < \overline{\varphi}_n(\vec{x}, E) >_{\vec{x},g} \cdots - \sigma_{n-1,g} < \overline{\varphi}_1(\vec{x}, E) >_{\vec{x},g}}{< \overline{\varphi}_o(\vec{x}, E) >_{\vec{x},g}} \tag{7d}$$

Where the subscript "g" represents integration over the energy range of group g. The above equations may be expressed in a monoenergetic formalism as:

$$\sigma_{x1} = \frac{<\sigma_x(\vec{r})\overline{\varphi}_1(\vec{r})> - \sigma_{xo}<\overline{\varphi}_1>}{<\overline{\varphi}_o>} = <\sigma_x(\vec{r})\overline{\varphi}_1(\vec{r})> \tag{8a}$$

$$\sigma_{x2} = <\sigma_x(\vec{r})\overline{\varphi}_2(\vec{r})> \tag{8b}$$

$$\vdots$$

$$\sigma_{xn} = <\sigma_x(\vec{r})\overline{\varphi}_n(\vec{r})> \tag{8c}$$

Dropping the group index for convenience, the discontinuity factor (Smith, 1986) is defined as the heterogeneous surface flux divided by the homogeneous surface flux for the assembly (node):

$$f \equiv \frac{\overline{\varphi}_s}{\phi_s} \tag{9}$$

The numerator of this ratio is determined from the heterogeneous core calculation and the denominator is found from the nodal (homogeneous) core calculation. Since neither of these fluxes is known a priori, the ratio is estimated as the surface flux to the assembly average flux from the infinite medium assembly calculation as would be given by the first term on the right hand side of Eq. (2). Rahnema and Nichita (1997) showed that *f* given by Eq. (9) could be decomposed into two ratios as given below:

$$f \equiv \chi \frac{\phi_{ave}}{\phi_s} \tag{10}$$

Here, $\phi_{ave}$ and $\phi_s$ are the node average and boundary fluxes determined from the core calculation. The heterogeneous discontinuity factor $\chi$ is defined as:

$$\chi \equiv \frac{\overline{\varphi}_s}{\overline{\varphi}_{ave}} = \frac{\overline{\varphi}_s <1>}{<\overline{\varphi}>} = \overline{\varphi}_s <1> \tag{11}$$

This factor may be expanded as in Eq. (2) and solved for using the high-order fluxes determined by the boundary condition perturbation theory.

The above analysis is summarized as follows. By using high-order boundary condition perturbation theory, the assembly-homogenized parameters required by nodal methods can be expanded in terms of the assembly (node) boundary current-to-flux ratio. The expansion coefficients are then computed by performing single assembly adjoint calculations with a zero-current boundary condition. With these coefficients known a priori, the nodal method can correct the infinite-medium homogenized parameters as it computes the node boundary current-to-flux ratios. The method does not require iteration between the core and assembly calculations and therefore is very efficient and practical. The accuracy of the method increases by increasing the order of the perturbation (expansion) with almost no computational penalty. This is because the expansion coefficients are simply integrals of the known quantities from infinite medium (assembly) calculations determined a priori.

The numerical development of this method is very general and basic for the most part. There are two areas of interest that warrant further discussion. The first is the solution to the Green's function adjoint, $\Psi_o^*$. The other is the basic bilinear nodal method used in this paper.

The Green's function adjoint is defined as the solution to

$$(H^* - \lambda_o F^*)\Psi_o^*(\vec{r},\vec{r}_o) = \delta(\vec{r}-\vec{r}_o) - \overline{\varphi}_o(\vec{r}_o) \tag{12}$$

$$a_o \frac{\partial \Psi_o^*(\vec{r},\vec{r}_o)}{\partial n} + b_o \Psi_o^*(\vec{r},\vec{r}_o) = 0, \vec{x} \in \partial V \tag{13}$$

with the uniqueness condition defined by

$$< \Psi_o^*(\vec{r},\vec{r}_o) F\overline{\varphi}(\vec{r}) >_{\vec{r}} = 0 . \tag{14}$$

In numerical methods, phase space must be discretized. In the multigroup case, the Green's function equation may be written as

$$(H_h^* - \lambda_o F_h^*)\Psi_0^*(\vec{x},h,\vec{x}_o,g) = \delta(\vec{x}-\vec{x}_o)\delta_{gh} - \overline{\varphi}_o(\vec{x}_o,g), h = 1,2,\ldots,g,\ldots G \tag{15}$$

$$a_o \frac{\partial \Psi_o^*(\vec{x},g,\vec{x}_o,h)}{\partial n} + b_o \Psi_o^*(\vec{x},g,\vec{x}_o,h) = 0, \vec{x} \in \partial V \tag{16}$$

where $g$ and $h$ are energy groups with $G$ maximum number of energy groups and $\delta_{hk}$ is the Kronecker delta function:

$$\delta_{hg} = \begin{cases} 1, h = g \\ 0, h \neq g \end{cases} \tag{17}$$

The adjoint diffusion and production operators, $H_h^*$ and $F_h^*$, are defined as

$$H_g^* = -\nabla \cdot D_g(\vec{x},E)\nabla + \sigma_{ag}(\vec{x}) - \sum_{g'=1}^{G} \sigma_{sgg'} \tag{18}$$

$$F_g^* = \nu_g \sum_{g'=1}^{G} \sigma_{fgg'} \tag{19}$$

For completeness the diffusion operators (which determine the normalized flux) are given below:

$$H_g = -\nabla \cdot D_g(\vec{x},E)\nabla + \sigma_{ag}(\vec{x}) - \sum_{g'=1}^{G} \sigma_{sgg'} \tag{20}$$

$$F_g = \sum_{g'=1}^{G} \nu_{g'} \sigma_{fg'g} \tag{21}$$

In the one-dimensional monoenergetic model used in this paper, Eqs. (15) and (16) may be set up in a tridiagonal matrix for each $\vec{x}_o$ and solved using standard numerical techniques. However, these techniques fail since the solution is not unique and Eq. (14) must be accounted for. One possible solution is to modify the tridiagonal matrix in the row where $\vec{x}$ is equal to $\vec{x}_o$. Replacing this row with the coefficients taken from the discretized form of Eq. (14) gives a solvable matrix system that has a unique solution.

A description of the bilinear coarse-mesh method used in testing the homogenization method is given in Appendix A.

## III. RESULTS

The new homogenization method is tested by considering two seven-assembly configurations typical of a BWR core in 1-D as shown in Fig. 1

FIGURE 1
Core Layout Configurations

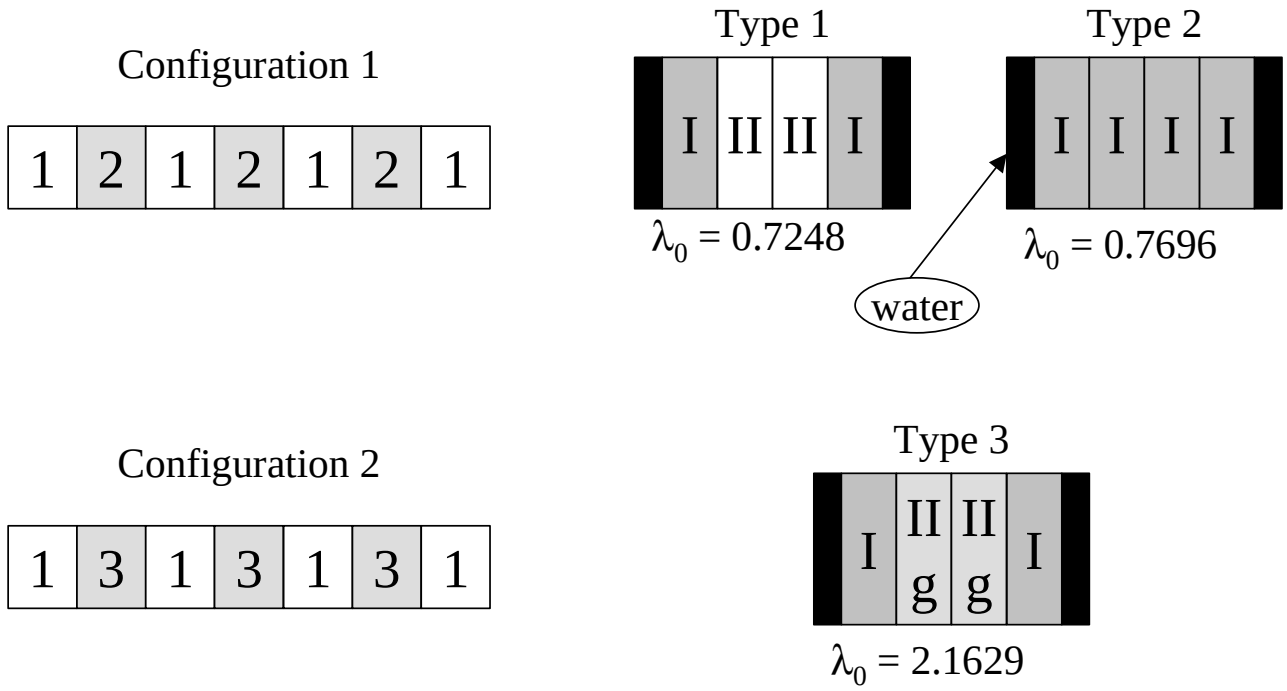


A seven-assembly core is made up of two unique alternating assemblies lined up in a one-dimensional array with a zero-current external boundary condition. The type 1 assembly contains two enrichment zones where as the type 2 assembly has one enrichment zone with slightly smaller average enrichment. The type 3 assembly is the same as type 1 except that it contains gadolinium in fuel region II. The gadolinium content is purposely increased by a substantial amount to create a highly heterogeneous configuration. The first configuration is a very simple case with relatively small changes across the core. The second configuration is designed to be a relatively difficult benchmark problem for coarse-mesh methods. The core and the assembly configurations are shown in Fig. 1 above. The corresponding cross sections and dimensions used for each region are shown in Table 1.

TABLE 1
Fuel Assembly Parameters

| Attribute | Water | Fuel I | Fuel II | Fuel IIg |
|---|---|---|---|---|
| D (cm) | 1.44 | 1.24 | 1.22 | 1.30 |
| $\Sigma_a$ ($cm^{-1}$) | 0.00205 | 0.0238 | 0.0284 | 0.075 |
| $\nu\Sigma_f$ ($cm^{-1}$) | 0.0 | 0.0314 | 0.0416 | 0.00844 |
| Thickness (cm) | 1.158 | 3.231 | 3.231 | 3.231 |

We note that the test problems considered here are slightly different from those used by McKinley and Rahnema (2000). Here, for simplicity, the common regions in all three assemblies have the same cross sections instead of being slightly different..

We first test the accuracy of the homogenization method by itself through the more restrictive core configuration 2. The homogenization method will then be implemented into a bilinear coarse-mesh code to demonstrate how it improves the nodal results as the order of perturbation is increased. As postulated by the generalized equivalence theory, given the exact discontinuity and homogenized cross sections, the nodal results are independent of the intranodal flux shape. This will be demonstrated (verified) by using a flat (instead of a bilinear) flux shape in the coarse-mesh code. Finally, we'll show that the use of the high-order homogenization causes the coarse-mesh method to be superior to that using the standard GET parameters and a fine-mesh method to solve the nodal core problem. The fine-mesh homogenized results are referred to as the "best fit" model since the implicit intranodal flux shape is based on a fine-mesh calculation with homogenized nodes. We recognize these results as the best that current nodal methods can achieve.

The first test was to take each assembly from configuration 2 (the more restrictive example) and use boundary condition perturbation theory to determine the homogenization parameters for the exact albedos given from the reference case. A fine-mesh solution of the full core case was taken as the exact (reference) solution for the flux and eigenvalue. The exact eigenvalue is 0.8969. By using the exact flux distribution, the right and left face albedos for each assembly were determined. Only four of the seven assemblies in configuration 2 were considered due to symmetry. Using the unperturbed single assembly infinite medium (zero-current boundary condition) fine-mesh solution for assembly types 1 and 3, the high-order perturbation method was used to generate up to seventh-order values for eigenvalue, flux, and homogenized cross sections. Note that the infinite medium standard and adjoint Green's functions were also computed to determine the higher-order expansion coefficients given in Eq. (8). For the purpose of presenting the results, each assembly in the core is numbered sequentially from the left. The eigenvalue, flux and homogenized cross section results for each assembly are presented in Tables 2-5 below. The numbers in parentheses are the % errors of the perturbation method. The flux %RMS row compares the perturbation estimate of the flux to the exact value. Results for the heterogeneous discontinuity factor $\chi$ are presented in Tables 6-9.

TABLE 2
Analysis of Config. 2, Assembly 1* - Including Homogenized Cross Sections+

| | Unperturbed (Infinite-Medium) | First-Order | Second-Order | Third-Order | Exact |
|---|---|---|---|---|---|
| $\lambda$ | 0.7248 (19) | 1.0006 (-12) | 0.8414 (6.2) | 0.9230 (-2.9) | 0.8969 |
| Flux %RMS | 20.2 | 9.7 | 3.9 | 1.2[a] | - |
| D | 1.2616 (-0.22) | 1.2570 (0.14) | 1.2594 (-0.05) | 1.2583 (0.03) | 1.2588 |
| $\sigma_a$ | 0.02249 (1.5) | 0.02303 (-0.84) | 0.02275 (0.42) | 0.02288 (-0.16) | 0.02284 |
| $\nu\sigma_f$ | 0.03103 (1.8) | 0.03192 (-0.99) | 0.03145 (0.49) | 0.03166 (-0.18) | 0.03161 |

* Each assembly in the core is numbered sequentially from the left starting from the center assembly.
+ Type 1 Fuel Assembly with left and right albedo of 0 and 0.13321 respectively and 1200 meshes.
[a] $4^{th}$ order = 0.2

TABLE 3
Analysis of Config. 2, Assembly 2* - Including Homogenized Cross Sections+

| | Unperturbed (Infinite-Medium) | First-Order | Second-Order | Third-Order | Exact |
|---|---|---|---|---|---|
| $\lambda$ | 2.1629 (-141) | 1.4838 (-65) | 1.0805 (-20) | 0.8964 (-0.043) | 0.8968 |
| Flux %RMS | 56.6 | 9.8 | 7.6 | 5.7[a] | - |
| D | 1.2968 (0.32) | 1.2993 (0.13) | 1.3007 (0.023) | 1.3013 (-0.025) | 1.3010 |
| $\sigma_a$ | 0.03818 (-6.6) | 0.03686 (-2.9) | 0.03611 (-0.79) | 0.03579 (0.09) | 0.03582 |
| $\nu\sigma_f$ | 0.01765 (-1.2) | 0.01755 (-0.60) | 0.01748 (-0.22) | 0.01745 (-0.041) | 0.01744 |

* Each assembly in the core is numbered sequentially from the left starting from the center assembly.
* Type 3 Fuel Assembly with left and right albedo of -0.13321 and -0.00904 respectively and 1200 meshes.
[a] $4^{th}$ order = 0.3

TABLE 4
Analysis of Config. 2, Assembly 3* - Including Homogenized Cross Sections+

| | Unperturbed (Infinite-Medium) | First-Order | Second-Order | Third-Order | Exact |
|---|---|---|---|---|---|
| $\lambda$ | 0.7248 (19) | 0.9652 (-7.6) | 0.8680 (3.2) | 0.9081 (-1.2) | 0.89705 |
| Flux %RMS | 15.3 | 6.1 | 2.0 | 0.5[a] | - |
| D | 1.2444 (-0.19) | 1.2411 (0.081) | 1.2424 (-0.021) | 1.2419 (0.019) | 1.2421 |
| $\sigma_a$ | 0.02249 (1.5) | 0.02296 (-0.53) | 0.02279 (0.22) | 0.02286 (-0.060) | 0.02284 |
| $\nu\sigma_f$ | 0.03103 (1.8) | 0.03181 (-0.63) | 0.03153 (0.26) | 0.03163 (-0.072) | 0.03161 |

* Each assembly in the core is numbered sequentially from the left starting from the center assembly.
+ Type 1 Fuel Assembly with left and right albedo of 0.00904 and 0.10706 respectively and 1200 meshes.
[a] $4^{th}$ order = 0.09

TABLE 5
Analysis of Config. 2, Assembly 4* - Including Homogenized Cross Sections+

| | Unperturbed (Infinite-Medium) | First-Order | Second-Order | Third-Order | Exact |
|---|---|---|---|---|---|
| $\lambda$ | 2.1629 (-140) | 1.1407 (-26) | 0.9441 (-4.6) | 0.9092 (-0.77) | 0.9022 |
| Flux %RMS | 9.5 | 1.4 | 0.2 | 0.0[a] | - |
| D | 1.2968 (0.32) | 1.3005 (0.036) | 1.3012 (-0.013) | 1.3013 (-0.021) | 1.3010 |
| $\sigma_a$ | 0.03818 (-6.6) | 0.03619 (-0.99) | 0.03588 (-0.15) | 0.03585 (-0.041) | 0.03583 |
| $\nu\sigma_f$ | 0.01765 (-1.2) | 0.01750 (-0.29) | 0.01746 (-0.076) | 0.01745 (-0.033) | 0.01745 |

* Each assembly in the core is numbered sequentially from the left starting from the center assembly.
+ Type 3 Fuel Assembly with an albedo of -0.10706 on both sides and 1200 meshes.
[a] $4^{th}$ order = 0.0

TABLE 6
Heterogeneous Discontinuity Factor $\chi$ – Config. 2, Assembly 1*

| Perturbation Order | Boundary | | %Error | |
|---|---|---|---|---|
| | Left | Right | Left | Right |
| Exact | 1.1575 | 0.6297 | - | - |
| $0^{th}$ ($\infty$-medium) | 0.9907 | 0.9907 | -14.4 | 57.3 |
| $1^{st}$ | 1.2312 | 0.4475 | 6.4 | -28.9 |
| $2^{nd}$ | 1.1311 | 0.7090 | -2.3 | 12.6 |
| $3^{rd}$ | 1.1629 | 0.6023 | 0.5 | -4.4 |
| $4^{th}$ | 1.1584 | 0.6357 | 0.1 | 0.9 |
| $5^{th}$ | 1.1552 | 0.6309 | -0.2 | 0.2 |
| $6^{th}$ | 1.1586 | 0.6278 | 0.1 | -0.3 |
| $7^{th}$ | 1.1567 | 0.6311 | -0.1 | 0.2 |

* Each assembly in the core is numbered sequentially from the left starting from the center assembly.

TABLE 7
Heterogeneous Discontinuity Factor $\chi$ – Config. 2, Assembly 2*

| Perturbation Order | Boundary | | %Error | |
|---|---|---|---|---|
| | Left | Right | Left | Right |
| Exact | 2.2680 | 0.5942 | - | - |
| $0^{th}$ ($\infty$-medium) | 1.1664 | 1.1664 | -48.6 | 96.3 |
| $1^{st}$ | 1.9353 | 0.6895 | -14.7 | 16.0 |
| $2^{nd}$ | 2.2807 | 0.5132 | 0.6 | -13.6 |
| $3^{rd}$ | 2.3354 | 0.5324 | 3.0 | -10.4 |
| $4^{th}$ | 2.2835 | 0.5945 | 0.7 | 0.1 |
| $5^{th}$ | 2.2452 | 0.6203 | -1.0 | 4.4 |
| $6^{th}$ | 2.2483 | 0.6086 | -0.9 | 2.4 |
| $7^{th}$ | 2.2675 | 0.5902 | 0.0 | -0.7 |

* Each assembly in the core is numbered sequentially from the left starting from the center assembly.

TABLE 8
Heterogeneous Discontinuity Factor $\chi$ – Config. 2, Assembly 3*

| Perturbation Order | Boundary | | %Error | |
|---|---|---|---|---|
| | Left | Right | Left | Right |
| Exact | 1.0953 | 0.6917 | - | - |
| $0^{th}$ ($\infty$-medium) | 0.9907 | 0.9907 | -9.6 | 43.2 |
| $1^{st}$ | 1.1471 | 0.5705 | 4.7 | -17.5 |
| $2^{nd}$ | 1.0794 | 0.7346 | -1.5 | 6.2 |
| $3^{rd}$ | 1.0983 | 0.6794 | 0.3 | -1.8 |
| $4^{th}$ | 1.0953 | 0.6941 | 0.0 | 0.3 |
| $5^{th}$ | 1.0946 | 0.6919 | -0.1 | 0.0 |
| $6^{th}$ | 1.0955 | 0.6914 | 0.0 | -0.1 |
| $7^{th}$ | 1.0950 | 0.6920 | 0.0 | 0.0 |

* Each assembly in the core is numbered sequentially from the left starting from the center assembly.

TABLE 9
Heterogeneous Discontinuity Factor $\chi$ – Config. 2, Assembly 4*

| Perturbation Order | Boundary | | %Error | |
|---|---|---|---|---|
| | Left | Right | Left | Right |
| Exact | 1.4300 | 1.4297 | - | - |
| $0^{th}$ ($\infty$-medium) | 1.1664 | 1.1664 | -18.4 | -18.4 |
| $1^{st}$ | 1.3861 | 1.3862 | -3.1 | -3.0 |
| $2^{nd}$ | 1.4235 | 1.4235 | -0.5 | -0.4 |
| $3^{rd}$ | 1.4291 | 1.4292 | -0.1 | 0.0 |
| $4^{th}$ | 1.4299 | 1.4299 | 0.0 | 0.0 |
| $5^{th}$ | 1.4299 | 1.4300 | 0.0 | 0.0 |
| $6^{th}$ | 1.4299 | 1.4300 | 0.0 | 0.0 |
| $7^{th}$ | 1.4299 | 1.4300 | 0.0 | 0.0 |

* Each assembly in the core is numbered sequentially from the left starting from the center assembly.

The exact eigenvalue for each case in Tables 2-5 is obtained by performing the single assembly fine-mesh calculation with the computed albedos. It does not match the exact eigenvalue of the core due to numerical limitations in determining the albedo and in computations. The type-3 fuel assemblies (Table 8) have a larger absorption cross section due to the presence of gadolinium leading to an exact solution that is far from an unperturbed zero-current solution. This in turn leads to a larger error in the locations where type-3 assemblies reside as compared to type-1 fuel assembly locations in the core. Due to the assembly symmetry, assembly locations 1 and 3 as well as 2 and 4 have the same values in the exact column. The "flux %RMS" in Tables 2-5 is defined as

$$\text{Flux \%RMS} = 100\left[\frac{1}{N-1}\sum_{i=1}^{N}\left[(y_{exact,i} - y_{computed,i})/(y_{exact,i})\right]^2\right]^{1/2} \tag{22}$$

where $y$ stands for the flux at fine-mesh point $i$.

As seen from Tables 2-9, the accuracy improves with increasing order of the expansion terms. The fourth-order expansion (see footnotes to Tables 2-5) seems sufficient to significantly reduce the errors in the homogenized cross sections. The error in the heterogeneous discontinuity factor $\chi$ becomes insignificantly small when $7^{th}$ order perturbation theory is used (see Tables 6-9). The homogenized cross sections are global (volume averaged) parameters and therefore are less sensitive to neutron leakage (boundary current-to-flux ratio) than is the discontinuity factor. The discontinuity factor is a local (surface) parameter and therefore expected to be highly sensitive to the surface leakage as seen from the results in Tables 6-9.

The next test we performed was to set up a bilinear nodal method while correcting the discontinuity factor and cross sections with boundary condition perturbation theory as described in the previous section. Using the infinite medium (zero-current) boundary condition, the adjoint flux from Eqs. (12) and (13), with $a_o$=-$D$ and $b_o$=$0$, the forward flux and the standard homogenized parameters for assembly 1, 2 and 3 are precomputed (prior to the nodal (core) calculation). A bilinear coarse-mesh code was developed (see Appendix A) to use the adjoint function as an additional homogenization parameter. The current-to-flux

ratios are solved for using the coarse-mesh bilinear equations and then Eqs. (5) and (6) are evaluated up to an arbitrary $n^{th}$ order. The cross sections and discontinuity factors are then determined through Eqs. (8) and (11), respectively. The inner iteration consists of using these computed homogenization parameters with the nodal equations to compute a coarse mesh flux shape and eigenvalue. The inner iteration converges the flux and the eigenvalue to within $10^{-6}$. The homogenization parameters are updated at each outer iteration. The outer convergence criterion is relatively weak. The eigenvalue and flux are converged to within 0.03.

The coarse-mesh code uses a bilinear flux shape with discontinuous flux across nodal boundaries. In the core case, we have 7 nodes with each node computing 3 flux points: the left side, center, and right side. The code is run with orders of perturbation up to fourth-order. The zeroth-order corresponds to using the standard GET homogenization parameters that are not adjusted with the current-to-flux ratio between the nodes. The zeroth-order reconstructed flux is calculated by modulating the infinite-medium ($0^{th}$ order) fine-mesh flux with the node average flux. The perturbation method uses Eq. (6) to determine the reconstructed fine-mesh flux. The code determines the eigenvalue, the nodal flux and the reconstructed flux as mentioned above. Table 10 shows how the eigenvalue changes as the order of perturbation increases for both configurations:

TABLE 10
Eigenvalue Computed by Perturbation Order

| Order | Config. 1 Eigenvalue (Error %)* | Config. 2 Eigenvalue (Error %)* |
|---|---|---|
| $0^{th}$ | 0.7423 (0.1) | 1.1073 (23) |
| $1^{st}$ | 0.7417 (0.0) | 0.8324 (-7.2) |
| $2^{nd}$ | 0.7418 (0.0) | 0.9196 (2.5) |
| $3^{rd}$ | 0.7418 (0.0) | 0.8876 (-1.0) |
| $4^{th}$ | 0.7418 (0.0) | 0.8976 (0.1) |
| Exact | 0.7417 | 0.8969 |

* Error = (value-exact) / exact

Table 10 shows that the first configuration converges very fast. By the first-order, the errors for the first configuration are lower than the fourth-order analysis of the second configuration. The results show that the infinite medium ($0^{th}$ order) case gives a highly inaccurate value for the second configuration. Even the first-order has about a 7 % error associated with it. High-order analysis must be used to capture enough of the terms to build up a reliable eigenvalue estimate based on the bilinear intranodal flux shape. The reconstructed flux and the bilinear node average flux also show similar trends as seen in Tables 11 through 15:

TABLE 11
Zeroth-Order Assembly Integrated Flux

| Assembly | Configuration 1 | | | Configuration 2 | | |
|---|---|---|---|---|---|---|
| | Nodal (Error %*) | Reconstructed (Error %*) | Exact | Nodal (Error %*) | Reconstructed (Error %*) | Exact |
| 1 | 1.002 (-5.0) | 1.056 (0.0) | 1.055 | 1.082 (-54) | 2.872 (21) | 2.370 |
| 2 | 0.997 (1.3) | 0.979 (-0.1) | 0.984 | 0.913 (39) | 0.250 (-62) | 0.658 |
| 3 | 1.002 (1.8) | 0.988 (0.3) | 0.985 | 1.057 (196) | 0.310 (-13) | 0.357 |
| 4 | 0.997 (4.9) | 0.947 (-0.4) | 0.950 | 0.898 (418) | 0.105 (-39) | 0.173 |

* Error = (value-exact) / exact

TABLE 12
First-Order Assembly Integrated Flux

| Assembly | Configuration 1 | | | Configuration 2 | | |
|---|---|---|---|---|---|---|
| | Nodal (Error %*) | Reconstructed (Error %*) | Exact | Nodal (Error %*) | Reconstructed (Error %*) | Exact |
| 1 | 1.055 (0.0) | 1.054 (-0.1) | 1.055 | 2.827 (19) | 2.823 (19) | 2.370 |
| 2 | 0.984 (0.0) | 0.983 (-0.1) | 0.984 | 0.453 (-31) | 0.454 (-31) | 0.658 |
| 3 | 0.985 (0.0) | 0.984 (-0.1) | 0.985 | 0.188 (-47) | 0.188 (-47) | 0.357 |
| 4 | 0.950 (0.0) | 0.949(-0.1) | 0.950 | 0.068 (-61) | 0.068 (-61) | 0.173 |

* Error = (value-exact) / exact

TABLE 13
Second-Order Assembly Integrated Flux

| Assembly | Configuration 1 | | | Configuration 2 | | |
|---|---|---|---|---|---|---|
| | Nodal (Error %*) | Reconstructed (Error %*) | Exact | Nodal (Error %*) | Reconstructed (Error %*) | Exact |
| 1 | 1.055 (0.0) | 1.054 (-0.1) | 1.055 | 2.281 (-3.8) | 2.281 (-3.7) | 2.370 |
| 2 | 0.984 (0.0) | 0.983 (-0.1) | 0.984 | 0.722 (9.8) | 0.720 (9.5) | 0.658 |
| 3 | 0.985 (0.0) | 0.984 (-0.1) | 0.985 | 0.381 (6.8) | 0.374 (5.0) | 0.357 |
| 4 | 0.950 (0.0) | 0.949(-0.1) | 0.950 | 0.200 (15) | 0.196 (13) | 0.173 |

* Error = (value-exact) / exact

TABLE 14
Third-Order Assembly Integrated Flux for Config. 2

| Assembly | Nodal (Error %*) | Reconstructed (Error %*) | Exact |
|---|---|---|---|
| 1 | 2.465 (4.0) | 2.487 (4.9) | 2.370 |
| 2 | 0.641 (-2.6) | 0.650 (-1.2) | 0.658 |
| 3 | 0.304 (-15) | 0.311 (-13) | 0.357 |
| 4 | 0.144 (-17) | 0.146 (-16) | 0.173 |

* Error = (value-exact) / exact

TABLE 15
Fourth-Order Assembly Integrated Flux for Config. 2

| Assembly | Nodal (Error %*) | Reconstructed (Error %*) | Exact |
|---|---|---|---|
| 1 | 2.382 (0.5) | 2.386 (0.6) | 2.370 |
| 2 | 0.666 (1.2) | 0.671 (1.9) | 0.658 |
| 3 | 0.360 (0.9) | 0.366 (2.7) | 0.357 |
| 4 | 0.175 (0.9) | 0.177 (2.2) | 0.173 |

* Error = (value-exact) / exact

Only the first four assemblies were shown due to symmetry. The assembly integrated flux is normalized so the core has a value of 7.0. As before, the errors steadily decrease as the order of perturbation correction is increased. This is not obvious as seen in the changes from second to third-order in Tables (13) and (14) for configuration 2. Overall, the system (total flux and eigenvalue) improves for each higher order, but individual assembly values may actually experience an increase in error. By the second-order, the results for the first configuration stopped changing so Tables 14 and 15 omit configuration 1. The reconstructed flux has about the same error as the bilinear nodal flux shape, which is expected. The shape of the bilinear nodal flux and the reconstructed flux gives some additional insight into the problem. Figures 2 and 3 show the nodal shape for each configuration. Figures 4 and 5 show the reconstructed flux.

FIGURE 2
Nodal Flux Shape by Order of Perturbation for Config. 1

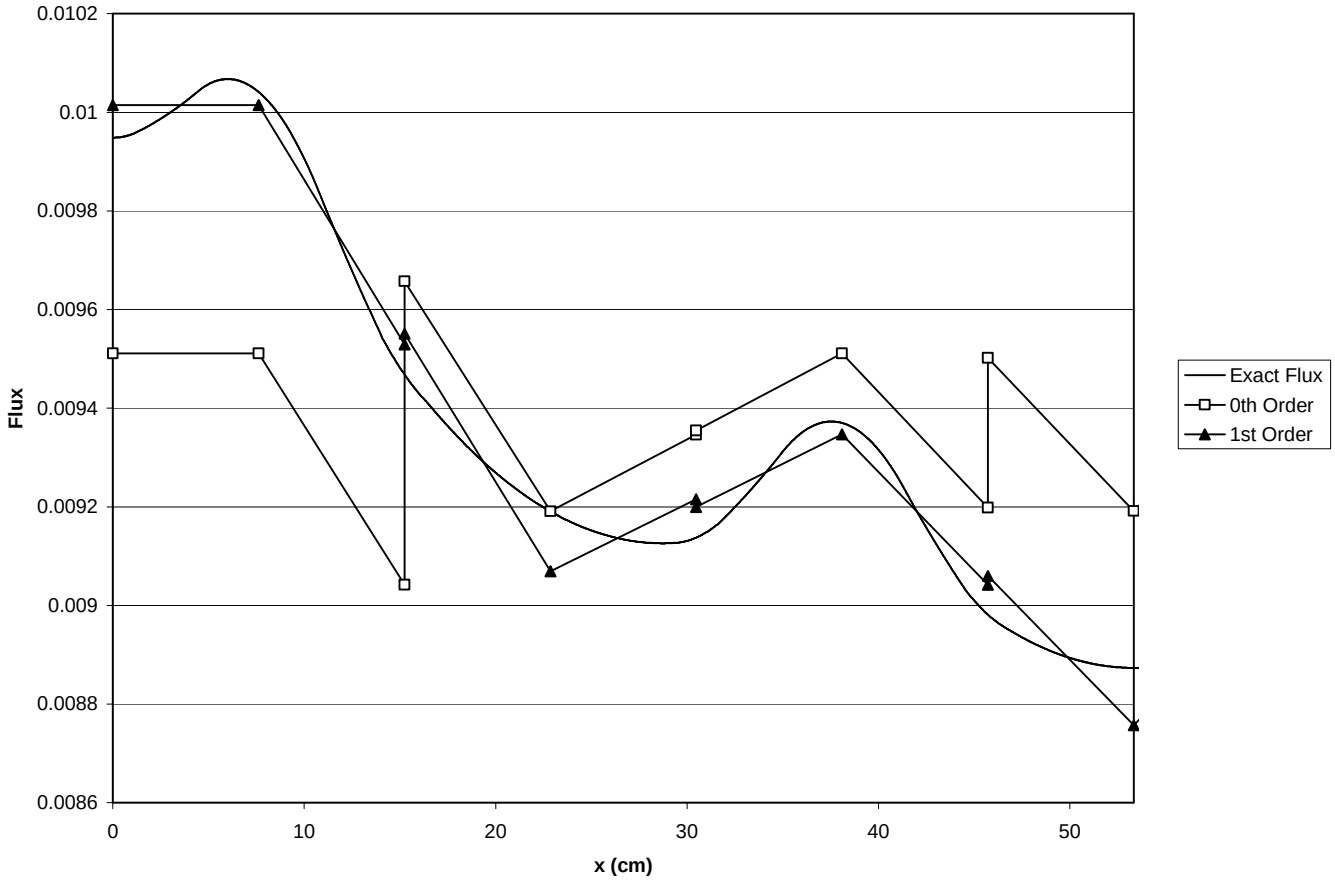

FIGURE 3
Nodal Flux Shape by Order of Perturbation for Config. 2

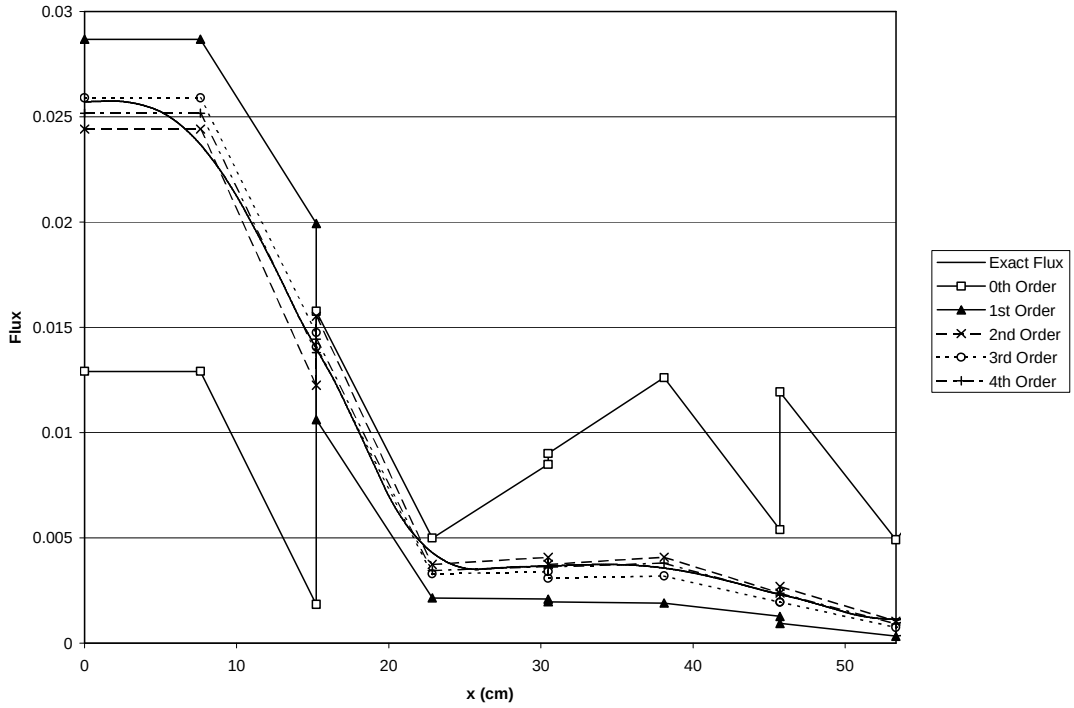


FIGURE 4
Reconstructed Flux Shape by Order of Perturbation for Config. 1

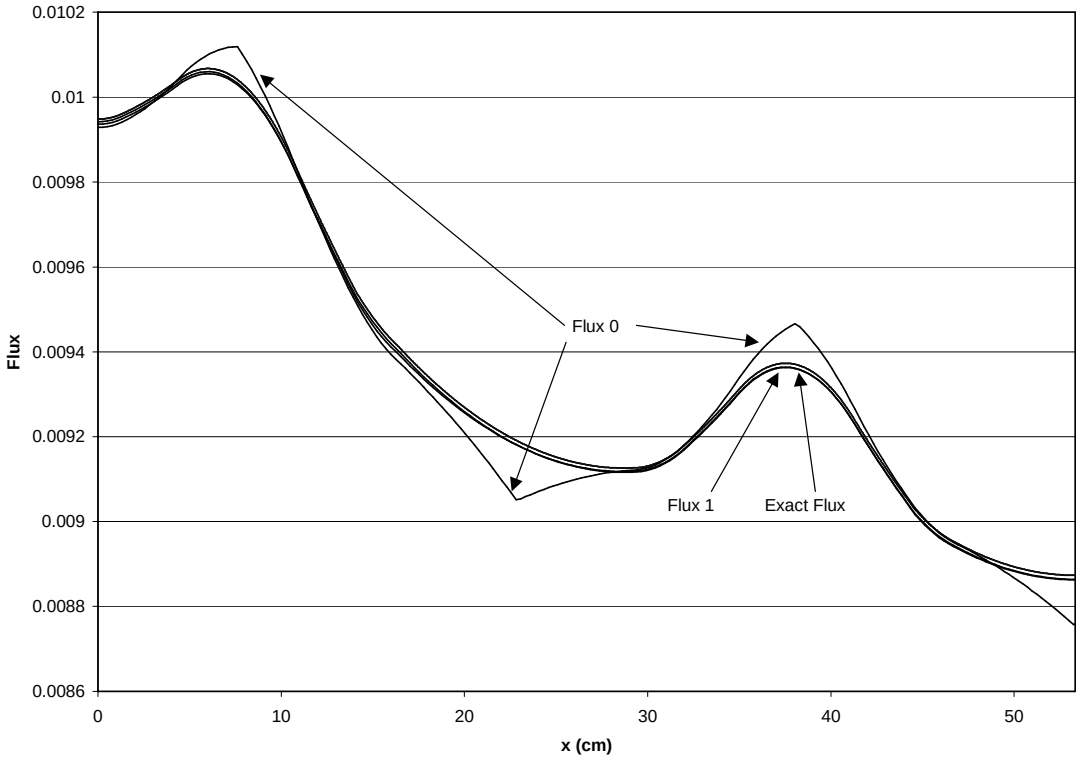

FIGURE 5
Reconstructed Flux Shape by Order of Perturbation for Config. 2

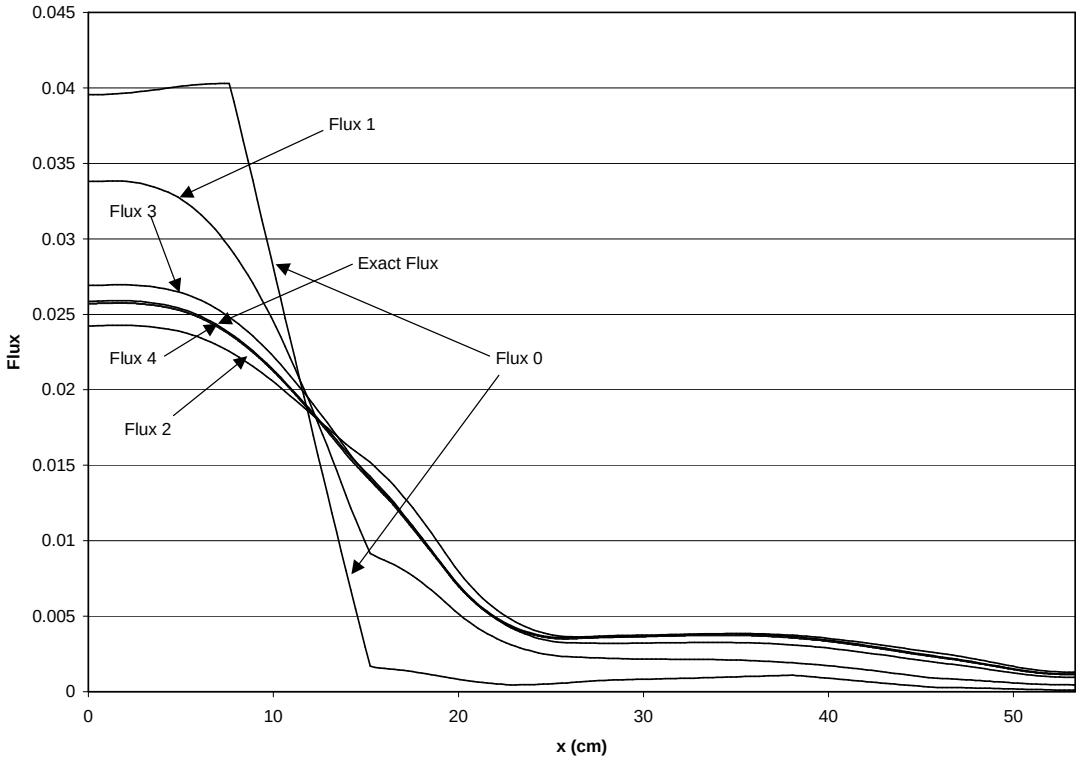


In the figures above, "Flux 0" represents the infinite medium ($0^{th}$ order) flux, "Flux 1" represents the flux to first-order, and so forth. As before, only half of the core configuration needs to be shown due to symmetry. In Figures 3 and 4, the nodal flux has two points at the assembly interface. This is due to the flux discontinuity assumption made by GET. The infinite medium homogenization parameters ($0^{th}$ order) yielded results that did not match the shape of the flux very well. This can be seen also in Figures 4 and 5 with the reconstructed infinite medium flux. In Figures 3-5, the successive order of perturbation yields flux shapes that closely match the exact flux, by the first-order for configuration 1 and by the fourth-order for configuration 2. While the bilinear nodal shape does very well just using three points to match the flux, the reconstructed flux shows how well the flux is being matched using the theory presented here.

In addition to modeling the nodal flux as bilinear, a separate coarse-mesh code was tested that models the flux as flat across a node. The central node flux is equal to the average flux in this model. While this model is much cruder and simpler than a bilinear flux shape, the average nodal flux and eigenvalue are very close in value to what the bilinear coarse-mesh model predicts for perturbations of first-order or greater. Also, the reconstructed flux matched very closely the bilinear reconstructed flux. This illustrates how the perturbation methods can improve upon and compensate for very crude coarse-mesh methods.

Another comparison of interest pertains to how well the high-order method presented in this paper compares to a highly accurate nodal method which we call a "best fit" model. To see this, we set up a model that involved using a fine-mesh grid of 1000 points inside each assembly. The infinite medium discontinuity factor was used on the assembly interfaces. The standard GET homogenized cross sections were also used inside each assembly. The case was run to tight convergence and the results were summarized in Table 16 and plotted in Figures 6 and 7 below.

TABLE 16
"Best Fit" Integrated Flux Analysis

| Assembly | Configuration 1 | | | Configuration 2 | | |
|---|---|---|---|---|---|---|
| | Best Fit | Error %* | Exact | Best Fit | Error %* | Exact |
| 1 | 1.055 | -0.04% | 1.055 | 2.420 | 2.09% | 2.370 |
| 2 | 0.985 | 0.05% | 0.984 | 0.604 | -8.17% | 0.658 |
| 3 | 0.985 | -0.01% | 0.985 | 0.391 | 9.71% | 0.357 |
| 4 | 0.951 | 0.06% | 0.950 | 0.168 | -2.96% | 0.173 |

* Error = (value-exact) / exact

FIGURE 6
Nodal Method Comparisons for Config. 1

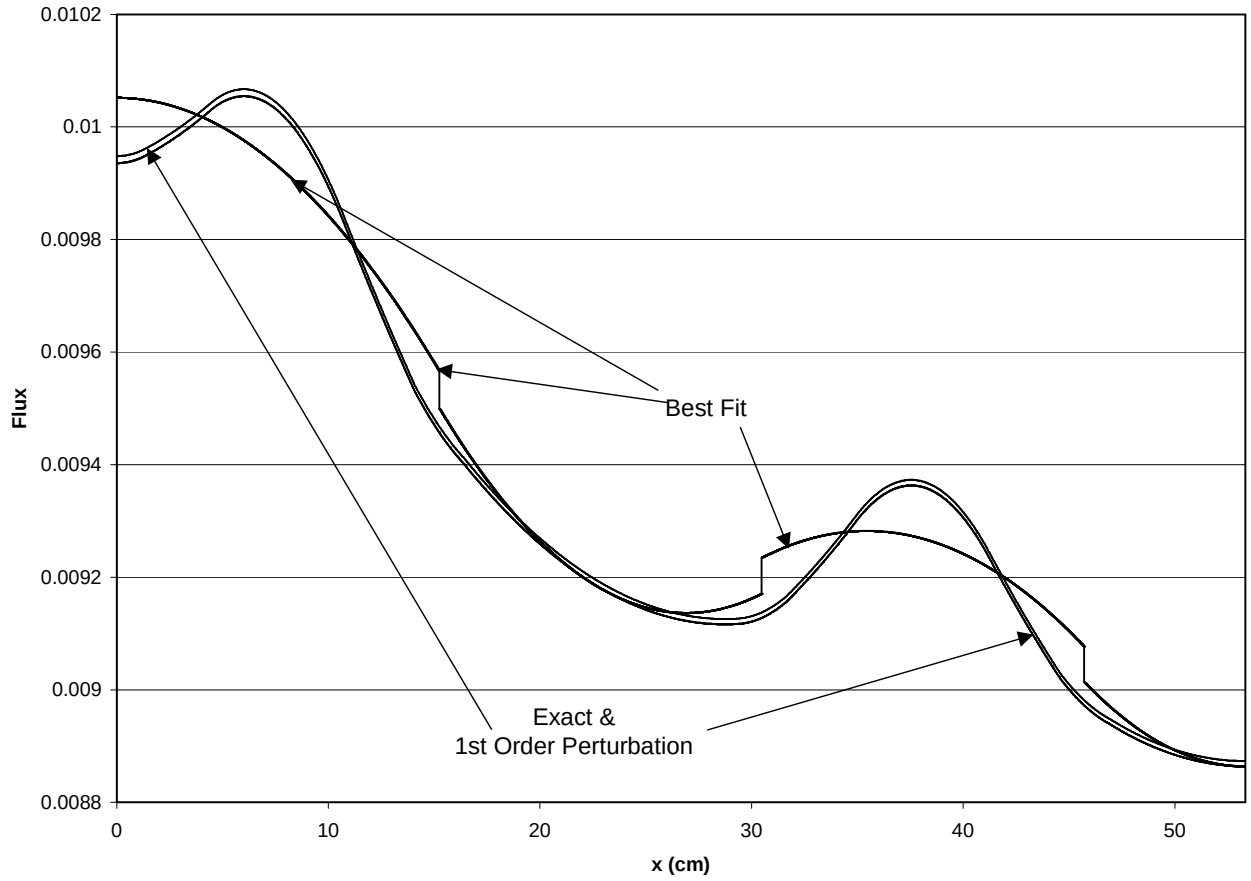


Figure 6 shows how well the first-order theory matches the exact flux versus the "best fit" model. The exact and fourth-order reconstructed fluxes lie on top of each other for the second configuration in Figure 7. While the "best fit" does very well for a nodal method, it does not capture all of the flux shape. The "best fit" model also predicts an eigenvalue of 0.7419 and 0.9007 for configurations 1 and 2, respectively. This gives an error of about 0.03% and 0.4%, respectively, while the first-order and fourth-order predictions for configurations 1 and 2 give an error of about 0.1%. The maximum error on the flux for both methods is summarized in Table 17. It can be seen that the maximum error in the reconstructed flux is reduced from 20% down to 3% for configuration 2.

We have shown that using the high-order homogenization method, one can improve the accuracy of the homogenized parameters including the discontinuity factor significantly. Therefore, it can be concluded that using the high-order method it is possible to develop a nodal method with very high accuracy.

FIGURE 7
Nodal Method Comparisons for Config. 2

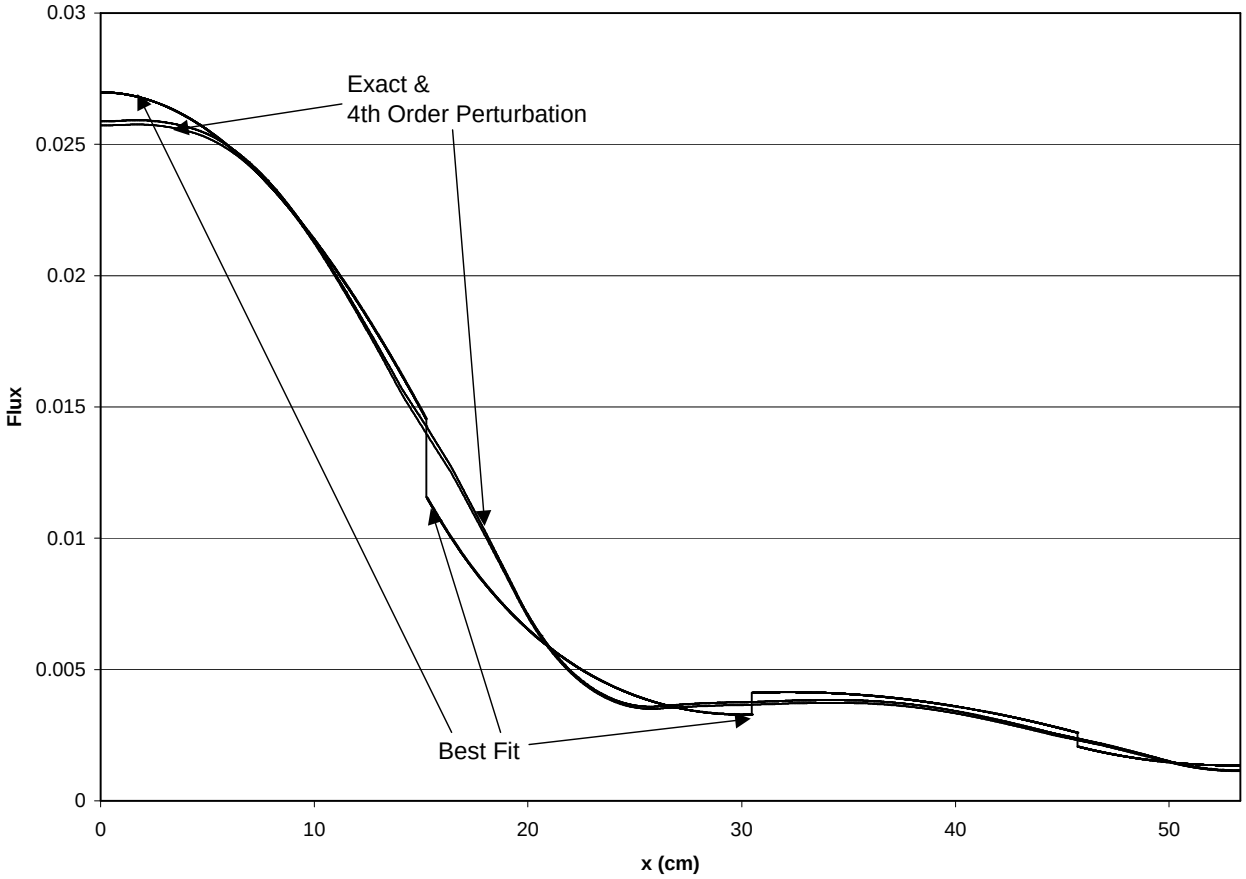


Table 17. Maximum %Error

| Method | Configuration 1 | Configuration 2 |
|---|---|---|
| Best Fit | 1 | 20 |
| High-Order Homogenization | 0.1 | 3 |

## IV. SUMMARY AND CONCLUSIONS

In this paper, a high-order homogenization method was developed based on the high-order boundary condition perturbation theory. The method expands the homogenized parameters in terms of the node (assembly) surface current-to-flux ratio. The expansion coefficients are then formulated in terms of the

known unperturbed solution to the infinite medium (zero boundary current) problem. In effect, the coefficients are precomputed just like the standard GET parameters. It was shown how to implement the homogenization method into a coarse-mesh method within the context of generalized equivalence theory.

It is shown that by using a homogenization technique based on high-order perturbation theory, it is possible to develop a nodal diffusion method that can almost reproduce the fine-mesh heterogeneous solution. The method is tested in one-speed diffusion theory using a highly heterogeneous BWR core in one-dimension. As expected, it is found that the accuracy of the method increases with increasing order of the perturbation for cases where the node-to-node leakages are "large." For the benchmark problems considered, errors of the coarse-mesh method become very small when higher-order perturbation is used in the expansion of the homogenized parameters.

The test performed on the reference BWR core highlights the accuracy improvements achieved with the high-order homogenization method that updates the homogenized parameters in a bilinear coarse-mesh code. The method also has the advantage that the reconstructed flux is a natural byproduct of the solution. We observed significant improvements in the flux and eigenvalue predictions as the order of perturbation increased. Although, first-order was satisfactory for configuration 1, a fourth-order analysis was needed to achieve similar accuracy for the highly heterogeneous configuration 2 given the bilinear intranodal flux shape. In addition, we showed that using a cruder intranodal flux shape (flat flux), which is computationally more efficient, the method still retains its accuracy. The results were also compared to a "best fit" approximation (fine-mesh homogenized node) that is considered as the most accurate solution from a nodal method based on the standard GET homogenized parameters. The high-order method was consistently superior.

The accuracy of nodal methods depends on the accuracy of the intranodal flux shape when standard GET parameters are used. For example, the accuracy of the nodal results would be improved if one uses high-order polynomial or an analytic flux shape instead of the bilinear shape. Of course, the computational efficiency would in turn suffer as one ends up with more coefficients in the nodal formulation. However, taking advantage of the theory of generalized equivalence, the high-order homogenization method can achieve the same high accuracy regardless of the intranodal flux shape. Of course, the higher the accuracy of the intranodal shape, the lower the homogenization order needed to achieve the same accuracy. However, since the method requires the same additional homogenization parameters regardless of the order used in correcting the standard parameters, increasing the order requires an insignificant increment in computational effort. Therefore, both the accuracy and the computational efficiency of nodal methods can be improved substantially by using the high-order homogenization method. Of course, the penalty paid for the improvement is the effort expended in precomputation of the additional homogenization parameters.

Based on the encouraging results from this paper, the next step would be to implement the high-order method into a multigroup multi-dimension nodal model.

## ACKNOWLEDGEMENTS

The work presented in the paper was supported by DOE through a NEER grant under DOE contract # DE-FG0-001D13960. Part of the research by the second author was performed under appointment to the Office of Civilian Radioactive Waste Management Fellowship program administered by the Oak Ridge

Institute for Science and Education under a contract between the U.S. Department of Energy and the Oak Ridge Associated Universities.

## REFERENCES

Calabrese, C. R., Grant, C. R. 1993. Use of Heterogeneous Finite Elements Generated by Collision Probability Solutions for Reactor Core. Ann. Nucl. Energy, 20, 117-127.

Chao, Y. A., Shatilla, Y. A., Ida, T., Tahara, Y. 1998 Challenges to Nodal Diffusion Methods for Cores with Mixed Oxide Fuel. Proc. Int. Conf. Physics of Nucl. Sci. and Tech., 1, 9, Long Island, New York.

Ellison, P. G., Lewis, E. E. 1983. A Coarse Mesh Element Method for Boiling Water Reactor Analysis. Adv. React. Comp. Proc. Meeting, Salt, Lake City.

Forslund, P., Muller, E., Lindahl, S-O. 2000. Intranodal Depletion Effects in MOX Cores. Proc. (CD) of PHYSOR 2000: ANS International Topical Meeting on Advances in Reactor Physics and Mathematics and Computations into the Next Millennium, Pittsburgh, USA, May 7-12, Am. Nucl. Soc.

Grummer, R., Lewis, C. Merk, S. 1997. The SAV 95 Code System for PWR Core Design. Proc. Am.Nucl. Soc. Topl Mtg.Advances in Nuclear Fuel Management II, 1**,** 5-47, Myrtle Beach, South Carolina March 23-26.

Hobson, G. H., Aigle, R. C. 1994. Nodal Code Developments at Framatome/BWFC. Topical Mtg. on Advances in Reactor Physics, Knoxville.

Iwamoto, T., Yamamoto, M. 1998. Development of a Multigroup Nodal BWR Core Simulator, NEREUS. Proc. Int. Conf. Physicsof Nucle. Sci. and Tech. 2, 1106, Long Island, New York.

Koebke, K. 1978, A New Approach to Homogenization and Group Condensation. IAEA-TECDOC 231, 303, International Atomic Energy Agency.

Koebke, K. 1081. Advances in Homogenization and Dehomogenization. Proc. Int. Topl. Mtg. Advances in Mathematical Methods for the Solution of Nuclear Engineering Problems, Munich, FRG, April 27-29, 1981, 2, 59, Kernforschungszentrum Karlsruhe.

Lawrence, R. D. 1986. Progress in Nodal Methos for the Solution of the Neutron Diffusion and Transport Equations. Prog. In Energy, 17, No. 2, 217 (1986).

Lindahl, S-O, Muller, E. Z. 1996. Status of ABB Atom’s Core Simulator POLCA. Proc. Int. Conf. Physics of Reactors, Mito, Japan.

Lee, C. H., Kim, Y. J., Song, J. W., Park, C. O., 1996. Incorporation of a New Spectral History Correction Method into Local Power Reconstruction for Nodal Methods. Nuc. Sci. Eng., 124, 160.

MCKINLEY, M. S., RAHNEMA, F. 1999. A Second-Order Accurate Eigenvalue Expression for Boundary Condition Perturbation. International Conference on Mathematics and Computation, Reactor Physics and Environmental Analysis in Nuclear Applications, Madrid, Spain, Sept. 27-30, Am. Nucl. Soc.

MCKINLEY, M. S., RAHNEMA, F. 2000. Higher-Order Boundary Condition Perturbation Theory for the Diffusion Approximation. Nucl. Sci. & Eng., 135, 15-33.

Moon, H. 1997. Advanced Core Design Using MICROBURN-B2 BWR Core Simulator. Proc.Am. Nucl. Soc. Topl. Mtg. Advances in Nuclear Fuel Management II, Myrtle Beach, South Carolina, March 23-26.

Mori, M. Kawamura, M. 1995. CASMO-4/SIMULATE-3 Benchmarking Against High Plutonium Content Pressurized Water Reactor Mixed-Oxide Fuel Critical Experiment. Nucl. Sci. Eng., 121, 41-51.

Nichita, E. M., Rahnema, F. 1998. A Finite Element Method for Boiling Water Reactors. International Conference on the Physics of Nuclear Science and Technology, Long Island, New York, USA, October 5-8, 1998, 1, 351, Am. Nucl. Soc.

Palmtag, S., Smith, K. S., 1998. Two-Group Spectral Corrections for MOX Calculations. Proc. Int. Conf. Physics of Nucl. Sci. and Tech. 1, 3, Long Island, New York.

Rahnema, F. 1989. Boundary Condition Perturbation Theory for Use in Spatial Homogenization Methods. Nucl. Sci. Eng., 102, 183-190.

Rahnema F., Nichita, E. M. 1997. Leakage Corrected Spatial (Assembly) Homogenization Technique. Ann. Nucl. Energy, 24, No.6, 477-488.

Rajic L., Ougouag, A. M. 1988. A Consistent Intranodal Burnup Correction Method for Advanced Nodal Depletion Analyses. Proc. Int. Reactor Physics Conference, III, 67, Jackson Hole, Wyoming.

SMITH, K. S. 1986. Assembly Homogenization Techniques for Light Water Reactor Analysis Prog. Nucl. Energy, 17, No. 3, 303.

SMITH, K. S. 1994. Practical and Efficient Iterative Method for LWR Fuel Assembly Homogenization. Trans. Am. Nucl. Soc., 71, 238.

Vogel D. L., Weiss, Z. J. 1992. A General Multigroup Formulation of the Analytic Nodal Method. Proc. Top. Mtg. Advances in Reactor Physics, Charleston, South Carolina.

Wagner, M. R., Koebke, K., Winter, H. J. 1981. A Nonlinear Extension of the Nodal Expansion Method. Proc. Int. Topl. Mtg. Advances in Mathematical Methods for the Solution of Nuclear Engineering Problems, Munich, FRG, April 27-29, **2**, 43, Kernforschungszentrum, Karlsruhe.

## Appendix A

The bilinear nodal flux shape used in this paper over an arbitrary node, *i*, can be seen in Fig. A-1. We first start with the diffusion equation as written below:

$$-\nabla \cdot D\nabla\varphi + \sigma_a \overline{\varphi} = \lambda \nu \sigma_f \overline{\varphi} = S \tag{A-1}$$

where $\overline{\varphi}$ is the flux averaged over a node. Since *D* does not change over a node, the first term may be written as a second derivative. Discretize the second derivative of the flux to get

$$\varphi_i^{"} = \frac{2\varphi_i^+ - 4\varphi_i + 2\varphi_i^-}{\Delta x^2}. \tag{A-2}$$

Since the discontinuity factor is the ratio of the heterogeneous surface flux to the homogenous surface flux, the continuity of the heterogeneous flux leads to

$$f_i^+ \varphi_i^+ = f_{i+1}^- \varphi_{i+1}^- \tag{A-3}$$

$$f_i^- \varphi_i^- = f_{i-1}^+ \varphi_{i-1}^+ . \tag{A-4}$$

Finally, the average flux is derived as

$$\overline{\varphi} = \frac{\varphi_i^+}{4} + \frac{\varphi_i}{2} + \frac{\varphi_i^-}{4}. \tag{A-5}$$

Using Eqs. (A-2 through A-5) in Eq. (A-1), we obtain

$$\frac{-D_i}{\Delta x_i^2}\left[\frac{2(\varphi_{i+1} + \xi^+\varphi_i)}{\xi^+ + \frac{f_i^+}{f_{i+1}^-}} - 4\varphi_i + \frac{2(\varphi_{i-1} + \xi^-\varphi_i)}{\xi^- + \frac{f_i^-}{f_{i-1}^+}}\right] + \sigma_a\left[\frac{\varphi_{i+1} + \xi^+\varphi_i}{4\left(\xi^+ + \frac{f_i^+}{f_{i+1}^-}\right)} - \frac{1}{2}\varphi_i + \frac{\varphi_{i-1} + \xi^-\varphi_i}{4\left(\xi^- + \frac{f_i^-}{f_{i-1}^+}\right)}\right] = S \tag{A-6}$$

where

$$\xi^+ = \frac{D_i \Delta x_{i+1}}{D_{i+1}\Delta x_i} \tag{A-7}$$

$$\xi^- = \frac{D_i \Delta x_{i-1}}{D_{i-1}\Delta x_i}. \tag{A-7}$$

Figure A-1
Bilinear Nodal Diagram